Further development and validation of CO_2FOAM for the atmospheric dispersion of accidental releases from carbon dioxide pipelines

Jennifer X Wen*, Pierre Le Fur, Hongen Jie and Vendra C. Madhav Rao
Warwick FIRE, School of Engineering, University of Warwick, Coventry CV4 7AL, UK
Corresponding author(s): Jennifer X Wen, Jennifer.wen@warwick.ac.uk

This paper reports on the further development and validation of CO_2FOAM, a dedicated computational fluid dynamics solver for the atmospheric dispersion of Carbon Dioxide (CO_2) from accidental pipeline releases. The code has been developed within the framework of the open source CFD code OpenFOAM® (OpenCFD, 2014). Its earlier version used the homogeneous equilibrium method for fully compressible two-phase flow. Validation of the code against CO_2 releases through vertical vent pipes and horizontal shock tubes was previously reported by Wen et al. (2013). In the present study, the homogeneous relaxation model has been implemented as it is more suited to account for the presence of solid CO_2 within the releases. For validation, the enhanced CO_2FOAM has been used to predict CO_2 dispersion in a range of full scale tests within the dense phase CO_2 PipeLine TRANSportation (COOLTRANS) research programme (Cooper, 2012) funded by National Grid. The test case used in the present study involved a puncture in a buried pipe. The experimental measurements were supplied to the authors after the predictions were completed and submitted to National Grid. Hence, the validation reported here is indeed 'blind'. The validated model has also been used to study the effect of a commercial building located downstream from the release location.

Key words: Carbon dioxide; Releases from pipeline accidents; Homogeneous Relaxation Model; Blind validation.

The COOLTRANS research programme is funded by National Grid in connection with the Don Valley Power Project which is co-financed by the European Union's European Energy Programme for Recovery. The sole responsibility of this publication lies with the authors. The European Union is not responsible for any use that may be made of the information contained therein.

Nomenclature

ρ	Density
U	Velocity vector
P	Pressure
k	Turbulent kinetic energy
ω	Specific dissipation rate
h_s	Sensible enthalpy
I	Identity tensor
σ	Surface stress tensor
Sc_t	Turbulent Schmidt number
Pr_t	Turbulent Prandtl number
g	Acceleration due to gravity
μ	Dynamic viscosity
μ_t	Turbulent viscosity
ν_t	Turbulent kinematic viscosity
β	Mass fraction of gaseous CO_2
α	Mass fraction of condensed phase CO_2
T_g	Gas phase temperature
τ	Relaxation time

Introduction

There is growing worldwide interest in Carbon Capture and Storage (CCS). CCS is a technology that prevents large quantities of Carbon Dioxide (CO_2) being released into the atmosphere from the use of fossil fuels in power generation and other industries. The realization of CCS often involves the

transportation of compressed CO_2 via high pressure pipelines and process systems often in the dense or super critical phases to ensure efficient high volume transportation capacity (Cooper, 2012). The need has hence arisen to address the potential loss of containment scenarios during the transportation process, as these could pose a risk to people and the environment. Although CO_2 might seem harmless, as it is present in the atmosphere at relatively low concentrations, it can cause serious health risks at higher concentrations (Mahgerefteh et al. 2011). Hence, it is important to assess such risks quantitatively so that appropriate guidelines can be developed to inform the development of pipelines for CO_2 transportation.

National Grid initiated the COOLTRANS (Cooper, 2012) research programme in 2010 to address knowledge gaps relating to the safe design and operation of onshore pipelines for transporting dense phase CO_2 from large industrial emitters in the UK to storage sites offshore. The University of Warwick was contracted to develop a mathematical model to predict the dispersion in the atmosphere that takes place if a buried pipeline transporting CO_2 is ruptured or punctured. This work forms part of COOLTRANS Work Package 1.4 on "Far Field Dispersion Studies". The work mainly involved numerical predictions of CO_2 dispersion in the far field taking into account obstacles, ground and gravity effects. It is recognised that for the simulation of the far field dispersion of the released CO_2 into the ambient environment, the gravity effect cannot be neglected due to the apparent density difference between the released CO_2 and the ambient air. Turbulence effect is of significant importance for jet dispersion downstream of the rapid expansion zone. The CO_2 jet entrains ambient air and any liquid/solid phase CO_2 at the exit will gradually vaporize/sublimate into gaseous CO_2 due to the mixing with ambient air. As such, the predictions of the correct fluid phase during the discharge and dispersion processes have received special consideration given the very different hazard profiles of CO_2 in the gas and solid states. In the collaborative COOLTRANS project [1], the analysis stages in the numerical study involves: (1) The group from University College London (UCL) to predict the outflow and conditions at the point of pipeline puncture; (2) The group from University of Leeds (UL) to predict the near-field conditions; and (3) Our group at University of Warwick (UW) predicts the far field dispersions using the boundary and initial conditions from UL. The present numerical simulations of the far field dispersion were started using the output from the near-field simulations of UL as boundary and initial conditions (Wareing et al., 2014). The dispersion process is affected by flow induced turbulence which leads to a high mixing rate between the released CO_2 and the ambient air. All these effects have been incorporated into the study along with the influence of wind, topography and obstacles to the releases. The detailed results of these parametric studies will be reported in a later paper although some snapshots are included here to illustrate the effect of obstacles.

The numerical method presented in this paper to simulate the dispersion of CO_2 in the far field follows several recently published works concerned with CO_2 dispersion. Some of them review by Dixon et al. (2012), most of these but not all are also research done within the context of CCS. Overall, the majority of these studies choose to solve a set of ensemble-averaged, density-averaged forms of the transport equations governing mass, momentum, and energy, involving full buoyancy terms (i.e. non-Boussinesq expression). These equations for averaged quantities are then complemented with a two-equation turbulence models (in most cases, standard k-epsilon). The studies concentrating on near-field especially tend to concentrate on handling the phase transition phenomena associated with accidental CO_2 releases. Wareing et al. (2013a, 2013b, 2014a, 2014b) tested both a Homogeneous Equilibrium model (HEM), and a Homogeneous Relaxation Model (HRM) to handle phase changes of CO_2. Closure of their equation set was achieved via the k–epsilon turbulence model, corrected to account for compressibility effects. Particular attention was given to developing a new equation of state for carbon dioxide (a composite equation using both Peng-Robinson and Span and Wagner equations). Importantly they noticed that their approach is valid, provided the CO_2 dense phase particles are sufficiently small. Their model is well validated against their own experimental observations on high pressure releases of multi-phase carbon dioxide "representative" of medium scale releases arising from an accidental pipeline puncture or rupture. In a similar approach Dixon et al. (2012) also tested both HEM and HRM with lagrangian particles for the solid and the inclusion of water condensation to simulate both horizontal and vertical releases (also using k-epsilon model). In both set of studies, comparison with near-field experimental data showed good agreements. Mazzoldi

et al. (2008, 2011) conducted quantitative risk assessment of scenarios involving CO_2 leakages for various CCS projects using PANACHE CFD code. They validated their model using Kit Fox experiments. These researchers focused on the far field results and on provision of an improved understanding of elements constituting the risk associated with an accidental release arising from the transport of the captured CO_2 from the industrial sources to a suitable storage site along high-pressure CO_2 pipelines by constructing hypothetical release scenarios. In both studies, the pipelines were assumed to be placed above ground level, and the downwind distance from the leakage source reached by a harmful concentration level (100,000 ppm or larger) of CO_2 was predicted and used to assess the risk to human health. Mazzoldi et al. (2008) simulated different release scenarios for CO_2 using both CFD (based on the Reynolds-averaged Navier–Stokes approach) and Gaussian plume models, and evaluated the predictive performance of these two approaches against two field experiments. They concluded (perhaps not surprisingly) that CFD models offered improved risk assessments for hazards associated with the dispersion of CO_2 clouds compared to the simpler Gaussian plume models. Recently Wen et al. (2013) also used the homogeneous equilibrium method to simulate both horizontal shock tube and vertical vent pipe cases. Uniform atmospheric BCs were assumed and roughness conditions were not taken into account. They also used a standard k-epsilon model. Similarly to previous researchers, good results were obtained when compared with experiments commissioned by National Grid with discrepancies within 25%. Xing et al. (2013) followed the same general approach using FLUENT. They again do not provide density modifications. Their validation is done with a reduced-scale field experiment designed to imitate a CO_2 blowout. Interestingly, they tested three different turbulence models: k-epsilon, RNG and SST. Results were in acceptable agreement with the experimental data (also using Hanna's statistical analysis) but noted that values found with the RNG model were unsatisfactory. Hsieh et al. (2013) simulated two scenarios: a storage tank release in the vicinity of a cubical obstacle and a pipeline rupture in a complex topography involving two axisymmetric hills. In their approach the density variations of the fluid (containing the dense gas) were simplified using the Boussinesq approximation. It's not clear whether such approach can be justified for near-field dispersion however, as the molecular weight of CO_2 markedly larger than air. Papanikolaou et al. (2011) conducted numerical simulations of CO_2 release to compare with experimental data taken from the Kit Fox CO_2 gas field experiments. Using ANSYS-CFX, it is not clear though which conservation equations they solve however, turbulence was modelled using the standard k-epsilon. Hedlund (2012) studied the real-world incident involving the catastrophic release of CO2 using the PHAST package to model the CO_2 outburst at the Menzengraben potash mine, where several thousand tons of CO_2 were blown out of a mine shaft. His numerical simulation results showed that in the case of the high momentum release, the leaked CO_2 diluted quickly and never reached the ground surface. In contrast, the low-momentum release resulted in a high concentration gas cloud near the ground surface.

Regarding initial and boundary conditions, Pontiggia et al. (2009, 2010) showed that better treatment of the upstream ABL, including stability classes, generates much better results for their simulations of Prairie Grass and Falcon tests. Scargiali et al. (2011) applies a k-epsilon model in urban area-style setting for heavy gas dispersion, first involving a stationary pre-release flow field simulation followed by a dynamic after-release flow and concentration field simulations. They used a so-called weakly compressible approximation for the buoyancy treatment instead of the simpler Boussinesq approximation employed elsewhere, in view of the strong density gradients in the proximities of the dense plume. The main hypothesis behind this approximation is that density variations are related only to the mean molecular weight and/or temperature changes in the fluid, while density is assumed to be independent of the pressure field, they thus assumed a reference pressure independent of density. Using chlorine, they found that the presence of buildings reduces the maximum ground concentrations while enlarging the affected area. Due to the larger negative buoyancy effects, increasing the amount of heavy-gas released slows down the cloud and increases (normalised) maximum concentrations and lateral spread of the cloud. While it proves quite difficult to establish general trends in the predictive abilities of the aforementioned modelling approaches. On the positive side, they are all capable (for all heavy gases) to predict the trends of the experiments within acceptable level of accuracy. Each provides a detailed picture of the flow and its interaction with the domain. They also serve as useful guides to what modelling approach to adopt.

Mathematical formulation and numerical framework

CO_2FOAM, a dedicated solver for CO_2 dispersion has been developed within the frame of the open source computational fluid dynamics code OpenFOAM® (OpenCFD, 2014). The code allows simulations with the relatively more efficient Steady or Unsteady Reynolds Averaged Navier-Stokes (RANS or URANS) approach as well as the more robust but computationally more intensive large eddy simulation (LES) approaches. It is known that the RANS approach which solves the time/density averaged transport equations is limited by the turbulence models. The LES approach aims at full resolution of the large, energy-bearing structures to momentum and energy transfer and only uses sub-grid scale models for the small eddies not resolved by the computational grids. Since the small scales tend to be more isotropic and universal in nature, their modelling is expected to be more amenable to success and require fewer adjustments when applied to different flows than models in the RANS approach. However, as the use of the LES approach will be computationally too expensive for the present study which involves relatively large computational domains and long durations, the majority of the simulations reported are conducted with the RANS approach with the k-ω SST turbulence model. In order to assess the potential loss of accuracy, preliminary predictions have been carried out with both approaches and found to show similar level of agreement with the experimental measurements. However, the LES predictions have captured the continuing rise in concentration after the cloud arrives at the probe whereas the RANS approach predicted an increasing gas turbulent diffusion. This suggests that the effect of density interface instability and turbulence damping are better captured by the LES. Quantitatively, the comparison shows that the differences in the predicted CO_2 concentration levels are only noticeable within the first 80 m from the release point, further from there, the RANS predictions are in reasonably good agreement with the mean values predicted by the LES approach. This has established the confidence in using the RANS approach when only the far field results of importance. The computational domain extends up to 250 m in the direction of the wind, capturing the far field dispersion.

All dense gas dispersion and heat transfer phenomena need to be included in atmospheric dispersion models used for predicting the dispersion of a CO_2 cloud formed from a pressurised release. Specifically, these include variable temperature and density, an appropriate turbulence model for dense gas dispersion, an adequate ground-level heat transfer model and gravity flow equations. It is also necessary to include atmospheric stability, complex terrain and source conditions. In order to reproduce field experiments for validation it may also be necessary to include time dependent wind speed and direction. The specification of appropriate inflow and surface boundary conditions, material properties and an appropriate turbulence model are hence crucial to the reliability of the predictions. The turbulence models, in particular, should include components which adjust for the damping effects of thermal or density stratification on turbulent generation and dissipation.

In the light of previous studies and experimental evidence (Mazzoldi et al. 2011 and Wareing et al. 2013), the approach undertaken by UW is in the first place to use the near-field predictions of Wareing et al. (2014) as the boundary and initial conditions for the far field simulations. Following on from the analysis conducted by Weber (2011), both the Homogeneous Equilibrium Method (HEM) and the Homogeneous Relaxation Model (HRM) should be applicable to the present applications. The earlier version of the CO_2FOAM code used the HEM approach to handle the fully compressible two-phase flow. Its validation against CO_2 release tests through vertical vent pipes and horizontal shock tubes was reported by Wen et al. (2013). In the HEM approach, the constituent fluid phases are assumed to remain at thermal and mechanical equilibrium during the decompression process. Consequently, phase-slip and non-equilibrium liquid/vapour transition phenomena, such as delayed bubble formation are ignored (Zucrow and Hoffman, 1975).

The HRM approach has been implemented into CO_2FOAM in the present study. In this approach, the assumption of mechanical equilibrium, i.e. no phase slip, is retained. However, non-equilibrium liquid–vapour transition is accounted for by a relaxation to thermodynamic equilibrium following Downar-Zapolski et al., (1996) and Brown et al., (2013). The choice of the time constant for the HRM also follows that of Brown et al. (2013). Although the pressure is lower than the CO_2 triple point

pressure at the immediate vicinity of the release point, the framework assigned to Warwick team is the atmospheric dispersion away from the three-phase, quickly expanding stages in the near proximity of the release from the pipeline. The HRM is hence adequate to model the mixture of solid and gas in such a far field dispersion study. The sizes of the solid CO_2 particles are assumed to be small enough so that modelling the CO_2 phase change as relaxation towards equilibrium composition holds. The deposition or rain out of dry ice is not handled in this model in the light of the reported inconsistent presence of deposited ice in experiments (GL, 2011).

Following previous researchers (Wen et al., 2013 and Hsieh et al., 2013), the RANS approach has been used to solve the three-dimensional conservation equations for a CO_2/air mixture for mean (ensemble-averaged) quantities in a turbulent flow field and are solved using governing equations being shown in the following section.

The Governing Equations

The compressible flow conservation equations are Farve averaged (mass weighted), any flow quantity f are split into mean and fluctuating component as $f = \tilde{f} + f''$ with $\tilde{f}'' = 0$ and $\tilde{f} = \frac{\overline{\rho f}}{\bar{\rho}}$. The ($\bar{f}$) overbar quantity represents Reynolds averaged mean quantity.

Continuity

$$\frac{\partial \bar{\rho}}{\partial t} + \nabla \bullet \bar{\rho} \tilde{U} = 0 \tag{1}$$

Momentum

$$\frac{\partial \bar{\rho} \tilde{\mathrm{U}}}{\partial t} + \nabla \bullet \bar{\rho} \tilde{\mathrm{U}} \tilde{\mathrm{U}} = -\nabla \bar{P} - \nabla \bullet \sigma + \bar{\rho} g \tag{2}$$

Where

$$\sigma = \left(\mu + \mu_t\right)\left(\nabla \tilde{\mathrm{U}} + \nabla \tilde{\mathrm{U}}^{\mathrm{T}}\right) - \frac{2}{3}\left(\mu_t \nabla \bullet \tilde{\mathrm{U}} \mathrm{I} + \bar{\rho} \tilde{k}\right) \tag{3}$$

In the treatment of buoyancy forces, the large density variations expected from the presence of dry ice and the molecular weight of CO_2 means that the Boussinesq approximation often applied in atmospheric dispersion studies cannot be applied (Hsieh et al., 2013). To model the diffusivity/turbulent diffusion flux, by analogy with Fick's law, a gradient law is employed. The transport equation for the mass fraction of gaseous CO_2 -' β ' can be written as:

$$\frac{\partial \bar{\rho} \tilde{\beta}}{\partial t} + \nabla \bullet \bar{\rho} \tilde{\mathrm{U}} \tilde{\beta} = -\nabla \frac{\mu_t}{Sc_t} \nabla \tilde{\beta} - \tilde{\alpha} \frac{p_{v-} p_s}{\tau p_s} \tag{4}$$

A simple sub-model for the relaxation to equilibrium has been included, in which the temperature relaxation is ignored and the condensed phase mass fraction is simply given by:

$$\frac{\partial \bar{\rho} \tilde{\alpha}}{\partial t} + \nabla \bullet \bar{\rho} \tilde{\mathrm{U}} \tilde{\alpha} = -\nabla \frac{\mu_t}{Sc_t} \nabla \tilde{\alpha} - \tilde{\alpha} \frac{p_{v-} p_s}{\tau p_s} \tag{5}$$

where p_v is the vapour pressure, p_s is the saturation pressure and τ is a relaxation time taking value of 0.1 ms. Taking species mass diffusion into account, the turbulent viscosity (μ_t) is corrected with the turbulent Schmidt number (Sc_t).

Previous research on atmospheric dispersion has used a range of values for Sc_t between 0.3 and 1.4 depending on various factors including presence of obstacles. In the first instance a value of $Sc_t = 0.7$ was selected following Hassid (1983) for neutral atmospheric conditions. A default turbulent Prandtl number of 0.85 is applied.

Energy Equations

Finally, energy conservation in the system is considered through the sum of sensible-enthalpy and turbulent kinetic energy equation.

$$\frac{\partial\bar{\rho}\left(\tilde{h}_s+\tilde{k}\right)}{\partial t}+\nabla\bullet\bar{\rho}\tilde{\mathrm{U}}\left(\tilde{h}_s+\tilde{k}\right)=\frac{D\bar{P}}{Dt}+\nabla\bullet\frac{\mu_t}{\mathrm{Pr}_t}\nabla\tilde{h}_s+\nabla\bullet\frac{\mu_t}{Sc_t}\nabla\tilde{\beta}\left(\tilde{h}_{CO_2}-\tilde{h}_{air}\right)+Q_{sub} \quad (6)$$

where, h_s is the sensible enthalpy of the fluid $h_s=\sum_i Y_i h_i$, is the energy flux, Q_{sub} represents the volumetric heat sources for the heat transfer due to sublimation of solid CO_2 particles. The following assumptions apply to the study of the dispersing jet: the effect of body forces (i.e. Coriolis forces) has no relevance on the system energy. Energy dissipation due to viscous forces in gas flow under a turbulent regime may be neglected; energy sources due to compressibility effects are ignored, since large pressure differences are not expected inside the cell; and the heat flux accounts for the heat conduction and the heat flux due to species diffusion with different enthalpies.

The JANAF thermochemical tables[1] (NIST, 1990) are used to calculate the specific heat at constant pressure and the sensible enthalpy for each species. The temperature and density are calculated assuming a homogeneous mixture of ideal gases. The Sutherland (1983) model is used to account for the temperature dependence of the viscosity of each specie in the mixture:

$$\mu\left(T_g\right)=\frac{A_s\sqrt{T_g}}{1+T_s/T_g} \quad (7)$$

where the Sutherland-law constants, A_s and T_s, are obtained from the JANAF database (NIST, 1990).

The system of partial differential equations was solved numerically using a collocated, finite-volume method. Diffusive volume-face fluxes were discretized using a second-order accurate central differencing scheme. The advective volume-face fluxes were approximated using a second-order accurate limited linear scheme. The transient term was discretized using a fully implicit, second-order accurate three-time-level method described in Ferziger and Peric (1996). The PIMPLE algorithm was used to combine the momentum and pressure equations (OpenCFD, 2014). PIMPLE (PIso-sIMPLE) algorithm is merger of semi-implicit method for pressure linked equations (SIMPLE) by Patankar (1980) and pressure implicit with splitting of operation (PISO) by Issa (1986), SIMPLE algorithm in outer iteration is merged with the PISO algorithm as inner iterations to correct the velocity and pressure explicitly.

Turbulence modelling

A turbulence model is required to close the set of averaged transport equations in RANS simulations. A wealth of studies examining the different choice of turbulence models for the simulation of gas dispersion in the atmosphere with or without obstacles or complex terrains exist. Several models, namely the k-ω shear stress transport (SST), k-ε RNG and realizable k-ε have shown better results in different cases with some performing better than others in various conditions. However, these models are often tested for handling high turbulence flow and in particular separating flow around buildings. While Wareing et al. (2014) employed a compressibility-corrected k-ε model in their numerical simulations of the near field flows, no comparative studies have been reported for applications that are similar to the present study for all these models. Hence the previous recommendations need to be treated with caution in evaluating the suitability of the models for CO_2 dispersion.

In the present case density gradients are practically entirely related to concentration gradients, as thermal gradients contribution due to Joule-Thomson effects and atmospheric conditions are negligible in the relatively short domain. The model chosen must be able to capture correctly the phenomenon of gravity slumping associated with dense gas dispersion. Standard two-equations turbulence models, initially developed for constant-density flows, do not account for the turbulence generation or suppression due to buoyancy forces. Thus, to account for this variation in the density and production of turbulence due to buoyancy, a source term is added to both equations. The source

[1] The JANAF thermochemical tables are a comprehensive thermodynamic database for pure substances.

term is modelled by either the simple gradient diffusion hypothesis (SGDH) or the generalized gradient diffusion hypothesis (GGDH) (Daly et. al., 1970). The SGDH is based on the standard Boussinesq gradient diffusion concept. The main difference between the two methods is the inclusion of the cross-stream density variation in GGDH, whereas the SGDH models only include the streamwise density gradient for a vertical plume. The SGDH is found to under-estimate buoyancy-produced turbulence and offer little improvement from the standard SST formations while the GGDH was found to offer improved predictions (Kumar and Dewan, 2014 and Maele and Merci, 2006). To further evaluate the potential improvement in the predictions which can be achieved by the use of GGDH and improved wall functions, e.g. Apsley (2007) extended to arbitrary wall roughness.

In order to better capture the interaction between the dispersed CO_2 and the atmospheric specific boundary layer (ABL-specific), a compressible form of the k-ω SST turbulence model (Menter, 1994) is used in conjunction with ABL-specific wall-functions for turbulence modelling in the RANS approach. The SST model (Menter, 1993) is essentially a two-equation eddy-viscosity model. It combines the best of the k-ε and baseline k-ω models with ω being the turbulent frequency (Menter, 1993). The use of the k-ω formulation in the inner parts of the boundary layer makes the model directly usable all the way down to the wall through the viscous sub-layer. Hence, the SST k-ω model can be used as a low Reynolds number turbulence model without any extra damping functions. The SST formulation also switches to k-ε type behaviour in the free-stream and thereby avoids the common k-ω problem that the model is too sensitive to the inlet free-stream turbulence properties. A blending function F_1 is used that depends on the wall distance and flow conditions. The equations for k and ω are defined as follows:

$$\frac{\partial \bar{\rho}\tilde{k}}{\partial t} + \nabla \bullet \bar{\rho}\tilde{\mathrm{U}}\tilde{k} = \nabla \bullet (\mu + \sigma_{k1}\mu_t \nabla \tilde{k}) + P_k - \beta' \rho \tilde{k}\tilde{\omega} \tag{8}$$

$$\frac{\partial \bar{\rho}\tilde{\omega}}{\partial t} + \nabla \bullet \bar{\rho}\tilde{\mathrm{U}}\tilde{\omega} = \nabla \bullet (\mu + \sigma_{\omega 1}\mu_t \nabla \tilde{\omega}) + 2\left(1 - F_1\right)\sigma_{\omega_2}\rho \frac{1}{\omega}\nabla \tilde{k} \bullet \nabla \tilde{\omega} + \frac{\alpha_3}{\nu_t} P_k - \beta_3 \rho \tilde{\omega}^2 \tag{9}$$

with β', α_1, σ_{k1},$\sigma_{\omega 1}$, $\sigma_{\omega 2}$, α_3 and β_3, as empirical constants (Menter, 1994). Due to the baseline formulation that does not account for the transport of turbulent stress, the eddy-viscosity would be over-predicted when calculating the turbulent viscosity from k and ω. A limiter to the kinetic viscosity is introduced to obtain such transport behaviour:

$$\nu_t = \frac{a_1 \tilde{k}}{\max\left(a_1 \tilde{\omega}, SF_2\right)} \tag{10}$$

with

$$\mu_t = \rho \nu_t \tag{11}$$

F_2 is a blending function similar to F_1 that restricts the limiter to the wall boundary layer and S is an invariant measure of the strain rate. More details especially on the blending functions F_1 and F_2 can be found in (Menter, 1993).

As observed by Ayrault et al. (1998) in studying the effect of negative buoyancy on plumes, the phenomenon of gravity slumping is closely associated with dense gas dispersion. They found that although the post-obstacle dispersion behaviour of the plumes mimicked that of a passive gas, the spread and effect on gas concentration were clearly marked on the upwind side and in-between the obstacles. They also found that the turbulence and concentration statistics showed less root mean square (RMS) variations than for neutral conditions, indicating the damping effect of density gradient on turbulence and dispersion. In order to capture this effect, it is important to incorporate appropriate buoyancy modifications. Thus, to account for this variation in the density and production of turbulence due to buoyancy, a source term is added to both equations. The source term is modelled by two methods:

1. The simple gradient diffusion hypothesis (SGDH)

$$S_B = -\frac{\mu_t}{g}\frac{1}{\bar{\rho}^2}\nabla\rho.(\nabla P + \rho_\infty g)$$

2. The generalized gradient diffusion hypothesis (GGDH).

$$S_B = -\frac{3}{2}\frac{\mu_t}{g}\frac{1}{\bar{\rho}^2 k}(u'u'\nabla\rho)\bullet(\nabla P + \rho_\infty g)$$

The former is found to under-estimate buoyancy-produced turbulence while improved predictions were reported with the latter (Kumar and Dewan, 2014 and Maele and Merci, 2006). However, little information was found on the performance of these models in negative buoyancy situations. The SGDH model was used by previous authors (Scargiali et al., 2011) simulating heavy gas dispersion with non-negligible effects. It was hence decided to test both methods.

Experiments considered

The experiment considered is Case Study 3 in the COOLTRANS research programme. It involved a nominally steady release from the side of a length of horizontal, below ground pipe, that was kept filled with CO_2 in the dense phase. The experiment was carried out to study how a puncture in a below ground pipeline would behave. The test section had a bursting disk fitted to one side. This disk failed at a pressure of approximately 150 barg, releasing CO_2 into a pre-formed crater below ground. The rig was instrumented with pressure transducers and thermocouples and the pressure and flow rate in the charge line were measured. The configuration resulted in a quasi-steady flow through the opening on the side of the pipe into the pre-formed crater. Approximately 30 kg/s of CO_2 left the crater at a maximum velocity of around 23 m/s. Measurements were made of the concentration and temperature within the resulting CO_2 cloud, as it dispersed in the atmosphere. A cross-section of the pre-formed crater that was manufactured to reproduce the crater formed in one of the earlier puncture experiments are shown in figure 1 and the locations of the temperature and CO_2 sensors are shown in Figure 2. The release conditions are summarised in Table 1.

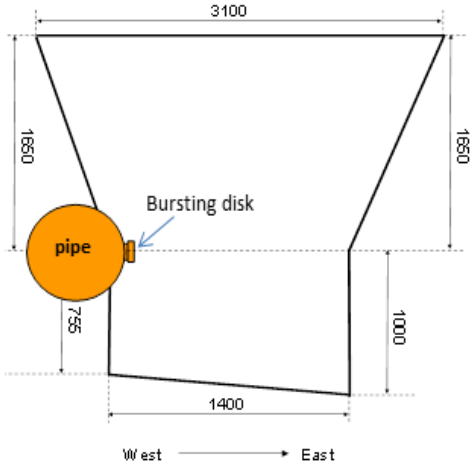

Figure 1. A cross-section (Elevation) of the preformed crater through the point of release constructed to surround the release location in Case Study 3 of the COOLTRANS research programme, dimensions in mm. (reproduced form Allason et. al., (2012)).

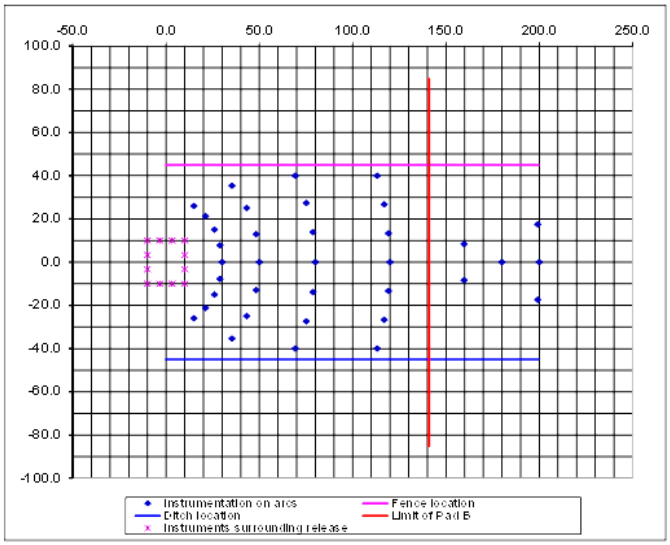

Figure 2. Locations of external temperature and concentration measurements in Case Study 3 of the COOLTRANS research programme (reproduced from GL (2011)).

Table 1: Initial Conditions for the puncture test (Reproduced from Wareing et al., (2014))

Section	**Item**	**Value**	
Release	Diameter of release	25	mm
	Outer diameter of test section	914	mm
	Wall thickness of test section	25.4	mm
	Depth of top of test section below local ground level	1.2	m
	Orientation of release	Horizontal at mid height of test section	
	Gas composition	Component	Mole %
		CO_2	100
Atmospheric and external conditions – average value in 30 seconds prior to test given	Temperature	3.6	^{o}C
	Relative humidity	81	%
	Average of wind speed measured at	0.73 at 4m 0.61 at 1m	m/s
	Average of wind direction measured at	255 at 4m 260 at 1m	o
	Surrounding terrain local to the point of release	Nominally flat	

Computational Set-up

In order to carry out full scale simulation of the field experimental trial, the crater inlet, atmospheric boundary conditions (wind) and ground conditions all need to be included in the model. The computational domain orientation is shown in figure 3.

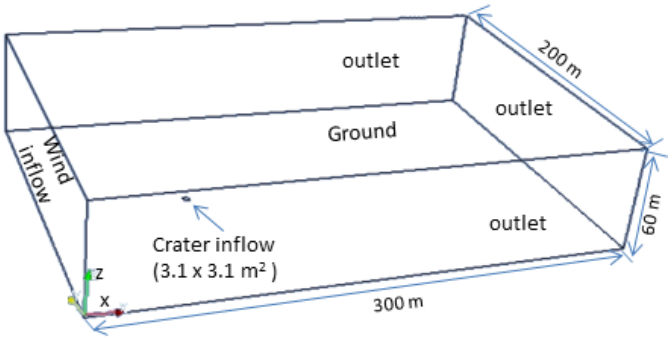

Figure 3. Computational domain

Crater inlet

In practice, risk analysts dealing with complex systems may have to apply a chain of numerical models, where the output of the first computation is used as input to the next one, etc. In this case, we can identify three particular release processes: in the pipeline, crater and atmosphere. As planned, the far field dispersion study has drawn upon the near-field dispersion studies by researchers at UL to provide inlet conditions while the computations of UL used the decompression simulations of the group from University College London. More specifically; the crater inlet data were taken from a concurrent study by Wareing et al. (2014), who simulated specifically the exit flow inside the crater corresponding to the rupture experiment. The UL's near-field predictions sampled from a plane at H = 0 was interpolated onto the computational domain in the present study to provide adequate boundary conditions for the CO_2 release from the crater. The crater inlets is placed at the ground level 80 m from upstream wind inlet and correspond to the origin of the frame. An unstructured mesh containing approximately 2.8 M cells with finer resolution around the crater inlet and the obstacle and coarser elsewhere.

The experiment showed that a high momentum jet of a mixture of air and solid/gas CO_2 escapes the crater. This highlights the importance of resolving this CO_2 source as opposed to using a point or simple area source often used in previous studies (Puttock, 1987). The released cloud carries significant momentum and this jet phase dominates its early dispersion, concurrently the air flow surrounding the crater is expected to be strongly affected by the release creating local recirculation and perturbing the equilibrium parabolic velocity profile set at the wind inlet. The details of this wind inlet are given in the following section. Another feature is the concentration of gas and solid CO_2 at the inlet. It is clear that a great deal of mixing took place within the crater and that the original dense phase CO_2 has expanded, resulting in a mixture of gaseous and solid CO_2 ejecting from the crater (Dixon et al. 2012, Mazzoldi et al. 2008 and Wareing et al. 2014).

The impact of the inlet conditions constitutes a certain departure from most other toxic gas dispersion studies in that the validity of the computational fluid dynamics (CFD) model is judged both on its ability to deal with the near-field and the more passive dispersion further outwards. Also important in the computational set-up is the specific toxicity of CO_2. Recent interest in CCS technology has prompted the reconsideration of the potential hazard of CO_2 in the context of potential very large release during CCS scale operation, which has the potential to produce a harmful effect (Engebø et al. 2013 and McGillivray et al., 2014). An important feature here is that the crater boundary also "sucks in" air from the atmosphere. When the flow thus exits this domain through the crater, zero gradient boundary conditions are set for the pressure.

Atmospheric and terrain Conditions

An aerodynamic surface roughness length of about 1 cm was determined to give the best fit to a logarithmic velocity profile, assuming a neutral stability atmosphere. That is the value of z_0 in the expression for the wind velocity profile below:

$$u(z) = \frac{u^* \log\left(z/z_0\right)}{k} \quad (12)$$

The atmospheric boundary layer at the inflow boundary is characterized by a velocity of 0.75 m/s at a 4 m height following a log-law (constant velocity boundary condition). The surface roughness length z_0 is 1.74 cm (chosen according to the terrain vegetation which is grass and bush covered) and the friction velocity u* is 0.8 m/s. The ambient air temperature is 283.15 K and humidity is 80%.

In order to model the atmospheric boundary layer (ABL), the inflow boundary conditions were chosen following the approach recommended by Richards and Hooxey (1993), Blocken et al. (2007) and Parente et al. (2011). This involved applying consistent boundary layer profiles for velocity corresponding to a neutral ABL (as indicated by the pressure gradient scheme). To be consistent with the inlet, the top boundary is set as a constant shear boundary. This implies that the top boundary should be high enough to be little disturbed by the crater release and/or obstacles.

Computations were conducted firstly to predict the steady-state atmospheric flow field with the area of the crater inlet treated as the ground. This flow field was then used as the initial condition for the subsequent predictions of the dense gas dispersion, which occurred when the gas mixture inside the crater was released to the atmosphere (time t = 0 s) by changing the crater boundary to CO_2 inflow. The interval of each time step was automatically adjusted during the computation to satisfy the Courant–Friedrichs–Lewy (CFL) condition of 0.1.

Wind direction is generally non-stationary and depending on meteorological conditions, may vary widely within a short period of time, i.e. a few minutes, in other words of the same order as an accidental release. Most previous CFD studies used a constant mean wind direction at inlet. However, this assumption as observed by Hanna et al. (1993), have led to previous RANS simulations of atmospheric dispersion showing a large discrepancy in lateral spread between simulations and experimental data. It also caused a significant overestimation of the concentrations in a vertical plane through the point of release and parallel with the wind direction. On the other hand, accounting for the full wind direction variability resulted in over-prediction of the lateral spreading of pollutants in some previous studies. It is, hence, thought that the measurements, which themselves are subject to the sensor response time and the actual readings, lie in between the constant wind and the variable-wind solutions.

Results and validation

Grid sensitivity study

The dimensions of the computational domain are 300 m (L) by 200 m (W) by 60 m (H). The X-axis is in the horizontal streamwise direction, i.e. parallel to the wind direction. The Y-axis is lateral and perpendicular to the wind direction while the Z-axis is in the vertical direction (shown in Figure 3). The CO_2/air mixture is released from the crater inlet at an approximate mass flow rate of 50 kg/s. All other sides (both lateral and downwind side), zero-gradient boundary conditions were chosen for the CO_2 mass fraction.

A grid sensitivity study has been conducted with three different mesh resolutions. The coarse, medium and fine meshes include 880,500, 2,577,040 and 5,792,900 grid points; respectively as shown in Table 2. Figures 4 and 5, illustrate that the predictions by the medium and fine meshes are almost identical. For the medium mesh the typical computational time was around 40 hours using 72 processor cores.

Table 2 Mesh attributes tested

	Points on inlet circle	Minimum dimensions (m)			Maximum dimensions (m)			Number of cells
		x	y	Z	x	y	z	
Coarse	50	0.20	0.20	0.30	4.58	4.00	2.35	880,550
Middle	80	0.12	0.12	0.25	3.23	2.85	1.85	2,577,040
Fine	100	0.098	0.098	0.20	3.05	2.22	1.34	5,792,900

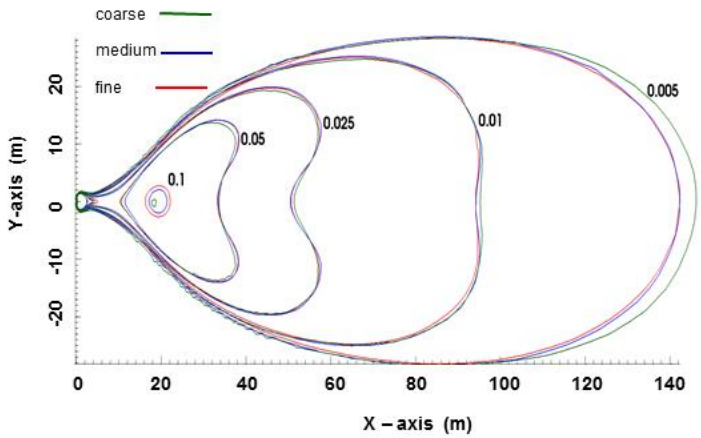

Figure 4. Comparison of the predicted CO_2 contours at ground level using different grid resolutions.

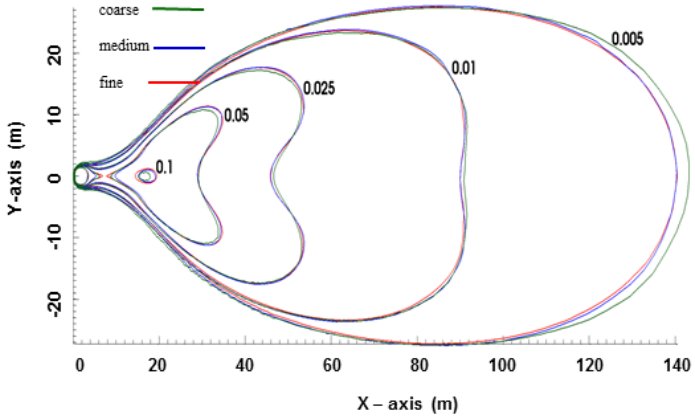

Figure 5. Comparison of the predicted CO_2 contours at 1m above ground using different grid resolutions.

In Table 3, the predictions with different grid resolutions for nine monitoring points are further compared, location of monitoring points are shown in Figure 6. It is seen that the largest differences between the predictions of the fine and medium resolutions is 6% for one point while for all other monitoring points the differences between the two sets of predictions are generally less than 2%. It was hence decided that the medium grid resolution will be used for the subsequent validation and parametric studies to investigate the effects of obstacles, slopes, wind speeds and directions. The first spacing is about 0.04 m and the grid size on the surface varies from 0.5 m close to the crater to 30 m in the far field. The maximum cell aspect ratio is 30, the maximum grid skewness is 1.2 and the mesh non-orthogonality is 10 (averaged) with a maximum of 40.

Table 3 Summary of the grid sensitivity study in percentage differences

Points	β at 3 m height			$\frac{\beta_{coarse}-\beta_{middle}}{\beta_{middle}}\%$	$\frac{\beta_{fine}-\beta_{middle}}{\beta_{middle}}\%$
	coarse	middle	fine		
A	0.062	0.063	0.062	-0.092	-2.06
B	0.014	0.013	0.014	+6.92	+6.02
C	0.016	0.016	0.016	+2.24	+0.18
D	0.018	0.019	0.018	-3.45	-1.67
E	0.010	0.010	0.010	+1.60	+0.43
F	0.007	0.007	0.007	-2.14	-1.09
G	0.007	0.007	0.007	+1.00	+0.44
H	0.007	0.007	0.007	+0.63	-0.01
I	0.005	0.005	0.005	+0.47	+0.45

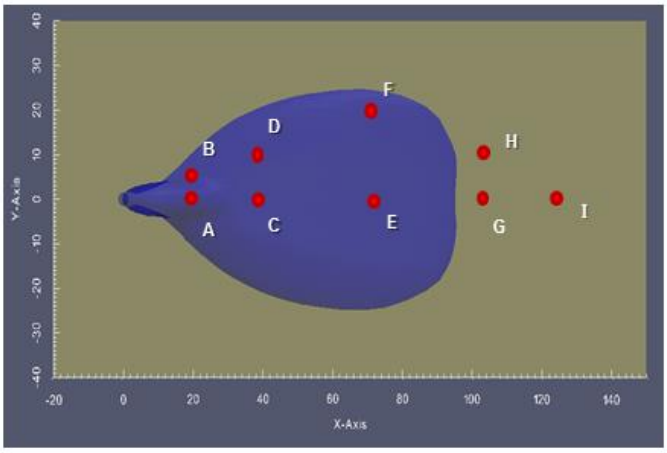

Figure 6. Monitoring point locations

Overall behaviour of the CO_2 cloud

Figures 7 (a) and (b), show the contours of 1% CO_2 concentration at different times after the dense gas cloud was released. The gravity slumping effect on the dispersion can be seen clearly in both figures, particularly at the earlier times where the flow vectors within the highly concentrated gas cloud exhibit a strong downward bulk motion. Initially the buoyancy generated forces and pressure gradients arising from density differences between the CO_2 gas cloud and its environment lead to a bulk motion that causes the dense cloud to spread in all directions near the release location (including a lateral spreading, as well as an upwind spreading against the prevailing wind direction).

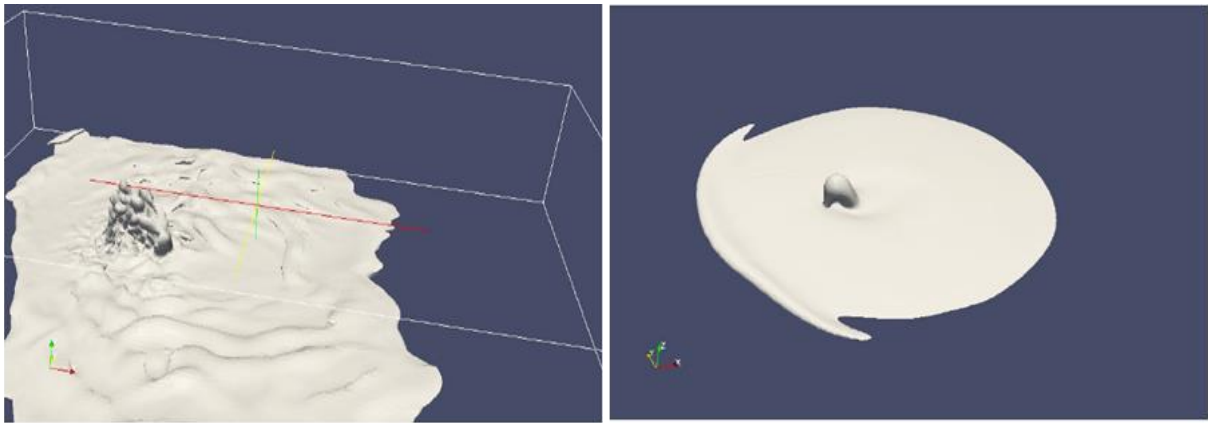

Figure 7. Overall view of mean concentration contours β = 1% at different times (a) earlier (71 s) and (b) later times (130 s).

Further downstream from the release, the bulk flow resulting from the gravitational slumping weakens as diffusion, mixing, and entrainment between the CO_2 gas cloud and the ambient air reduces the negative buoyancy effects of the cloud and strengthens the influence of the externally imposed velocity field on the transport and dispersion of the cloud. Whereas CO_2 was 'sprayed' upwards from the jet nozzle at an initial velocity and subsequently became rapidly diluted with the surrounding air, the initial velocity was still predominant resulting in the main tendency of CO_2 to move upwards, the 'spray' has a noticeable horizontal component of around 2 m/s in magnitude (i.e. the initial release is inclined to the crater wall at an angle of $\theta=70^0$). On top of the jet being inclined, the motion is expected to be affected by the wind coming across, however in this case, the wind being relatively of lower velocity, its motion was only slightly affected by it. The second phase of gravity slumping which marks heavy gas dispersion is most significantly different from that of a passive gas. Due to gravity, this phase was characterized by the slumping or collapse of the cloud towards the ground level. It continues to entrain ambient air, which resulted in a reduced density, i.e. a reduced density deficit. The loss of momentum of the jet is in a sense much faster than its dilution, creating the prevalence of gravity effects in the movement of the cloud. Subsequently, the CO_2 cloud dispersion goes into a third phase of gravity current, where the cloud pushes radially outwards, at a relatively steady speed. As the cloud volume grows wider and larger, it is further diluted by the ambient air. The decrease in concentration is gradual and the height of the CO_2 cloud decreased slightly. Finally, as the cloud density decreased, the negative buoyancy effects disappear and the CO_2 plume motion resembles that of passive gas.

Comparison between the measured and predicted CO_2 concentrations by different variations of the k-ω SST models and wall functions

To further evaluate the potential improvement in the predictions which can be achieved by the use of GGDH and improved wall functions extended to arbitrary wall roughness by Apsley (2007), predictions have been carried out for the Case Study 3-base case for the k-ω SST with GGDH, k-ω SST with the Apsley wall function and k-ω SST with both the GGDH and Apsley wall function. The predictions are shown in Figures 8 to 11, along with the experimental measurements. When examining the comparison with the measurements, one should bear in mind that the predictions are conducted with the pseudo source which approximate the outflow conditions when the release has reached quasi steady state. Hence one should not expect the predictions to capture the transient characteristics of the actual dispersion. However, the numerical simulation predicted some fluctuations in the concentration of CO_2 in the near fields, which can be attributed to the interplay between the jet momentum, buoyancy and the gravity. These fluctuations are almost negligible in the far field. Overall, the comparison indicates that although for some monitoring points the predictions by the k-ω SST with both the GGDH and Apsley wall function are in closer agreement with the base k-ω SST model, in the majority of the cases, the base k-ω SST model actually delivered predictions that more closely match the experimental data. The comparison supports our choice in using the base k-ω SST model for all the predictions and wall functions based on the roughness of the ground in the present study following Richards (1993).

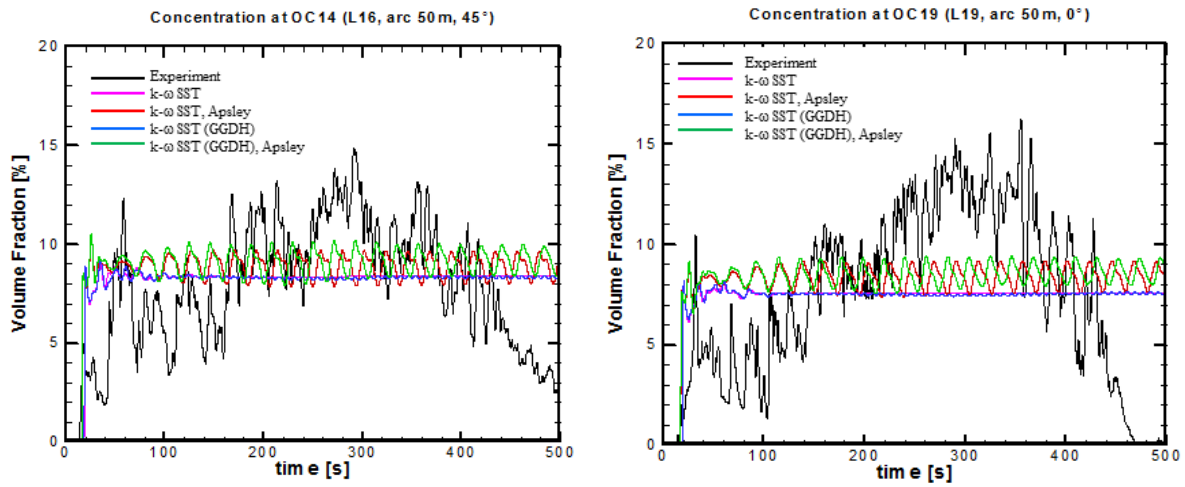

Figure 8. Comparison of the measured and predicted concentrations with different model combinations on the arc 50 m.

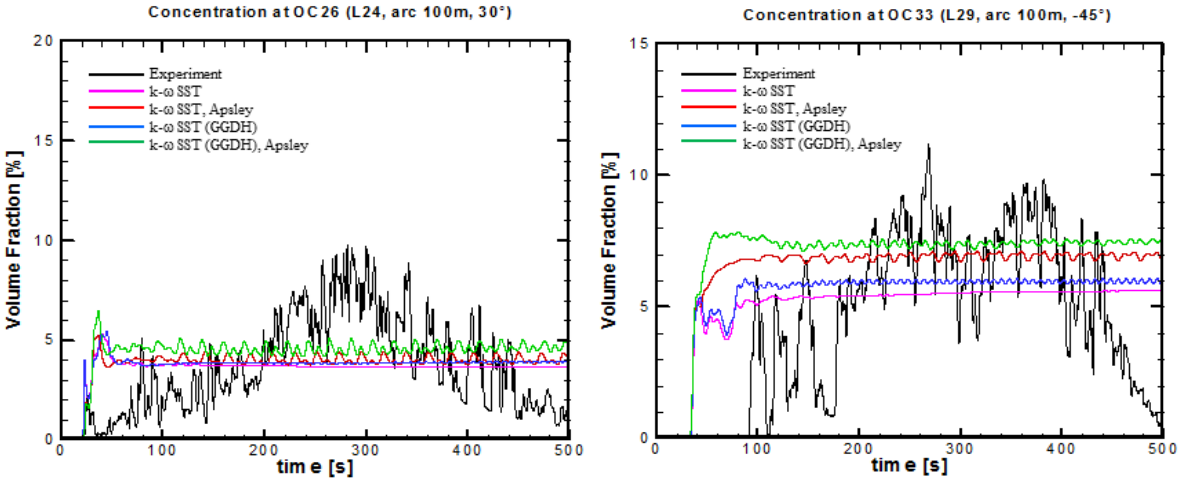

Figure 9. Comparison of the measured and predicted concentrations with different model combinations on the arc 100 m.

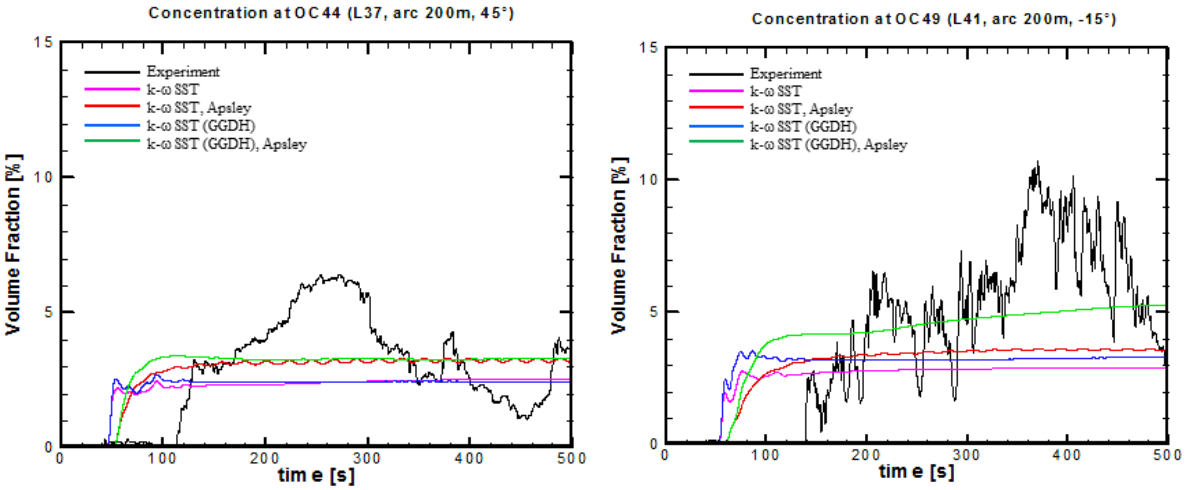

Figure 10. Comparison of the measured and predicted concentrations with different model combinations on the arc 200 m.

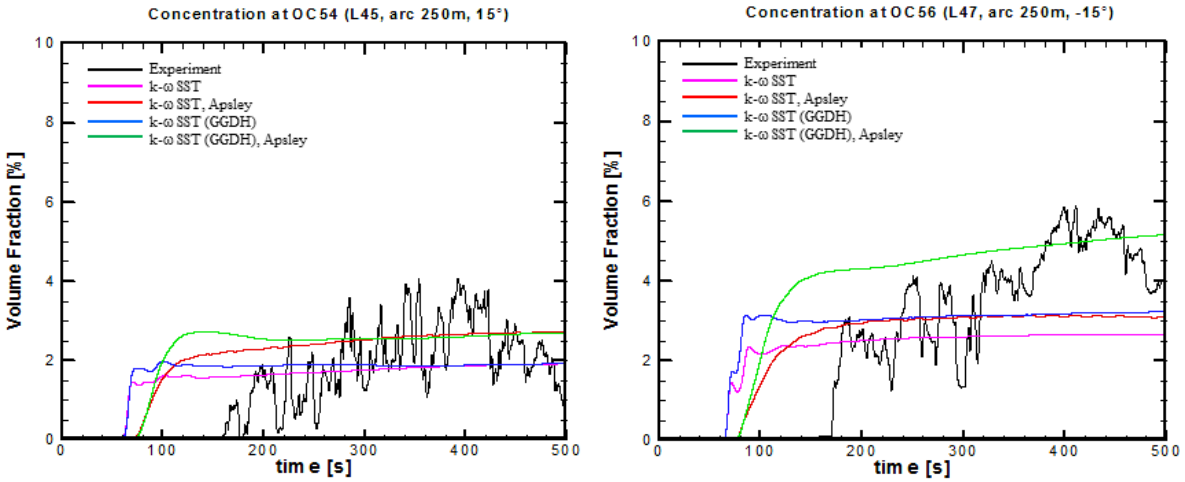

Figure 11. Comparison of the measured and predicted concentrations with different model combinations on the arc 250 m.

Further comparison between the measured and predicted CO_2 concentrations

As previously stated, the CO_2 concentration levels are of important concern in the safety context. A minimum value of interest could be as low as 1%, which can make some people feel drowsy. Generally, numerical predictions of concentration are seen to be in quite good agreement with the experimental data. It is noted that in interpreting the level of agreement between the predictions and the measurements, one needs to recognize that the measurements of the short time-averaged concentrations obtained correspond to one realization of the instantaneous dispersion, whereas the model predictions correspond to an ensemble-averaged concentration (and as such, is associated with an average over an ensemble of realizations of the instantaneous dispersion). Because the model prediction is compared to one realization out of the ensemble of all possible realizations, the discrepancy between the model predictions and the experimental measurements cannot be smaller than the expected fluctuations of the individual realizations about the ensemble mean. As a consequence, it is impossible for even a perfect model to give a greater precision in its predictions of the concentration than the expected concentration variability from realization to realization in the atmospheric dispersion. As shown in Figures 12 and 13 , both the predicted CO_2 volume fraction and the predicted and measured CO_2 concentration averaged over arcs by the RANS approach are in reasonably good agreement with the measurements. As noted by Clever et al. (2007) for the simulations of large scale dispersions of a liquefied natural gas spill, there appeared to be a degree of consensus that the better of the more, practical models (box or similarity models) should be within a factor of 2 of the observed concentrations for a straight-forward situation within the bounds covered by the experimental data. Similar comments were also reported by Hanna et al. (1993) and Daish et al. (2000). The agreement between the present predictions and the data averaged over the arcs are indeed within a factor of 0.5.

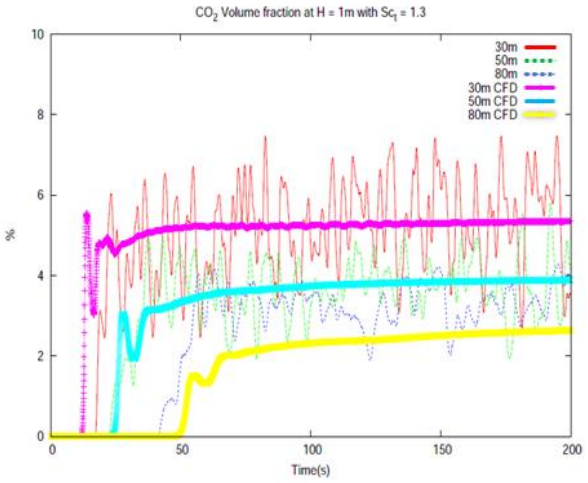

Figure 12. Comparison between the predicted and measured CO_2 volume fraction.

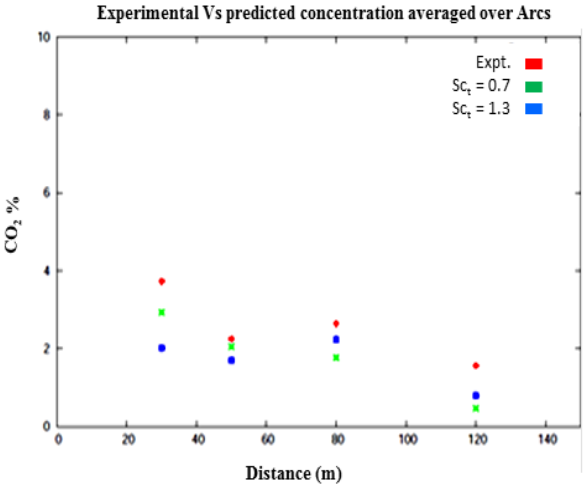

Figure 13. Comparison between the predicted and measured CO_2 concentration averaged over arcs.

Obstacle effects

A series of studies have also been conducted to investigate the effects of obstacles on CO_2 dispersion. While a more detailed paper about these studies is under preparation, some snapshots of results involving a commercial building using release conditions in Case Study 3 as the baseline release are included here to illustrate the application of the code. The commercial building is a single storey large building (representing a factory or warehouse) of dimensions 60 m wide by 30 m deep by 8 m high and placed with its front face 25 m downwind of the release. For simplicity, all windows or doors are assumed to be closed. The simulations were conducted for a wind speed of 1 m/s at a 10 m reference height. The simulations were conducted in two steps: the computations were run at first before the CO_2 was released to reach a steady-state atmospheric flow field. The flow field thus obtained was then used as the initial conditions to study the dispersion of CO_2 following the release.

The 2% iso-contours of CO_2 concentrations at t = 30 s and 300 s are shown in Figures 14 and 15 respectively. These overall views of the cloud show that the cloud wraps around the obstacle but not over it. In other words, high concentrations (1.5% and over) are contained or blocked by the commercial building which limits the spreading downstream of the obstacle but increases the spread laterally and upwind of the release point against the prevailing wind direction.

The commercial building also has considerable impact on the wind flow. Prior to the release, the buildings create a considerable velocity deficit in the atmospheric boundary layer, with recirculation zones lee- and wind-ward as well as to the side of the obstacle, the wind profile only returns to an equilibrium more than 50 m downwind. The recirculation zones are clearly illustrated by the streamlines shown in Figure 16. The interaction of the cloud with these recirculation patterns is most distinct in the decrease of the recirculation intensity and creation of the low velocity “calm” zones where the CO_2 can spread slowly (observe the flattened velocity profiles around the buildings).

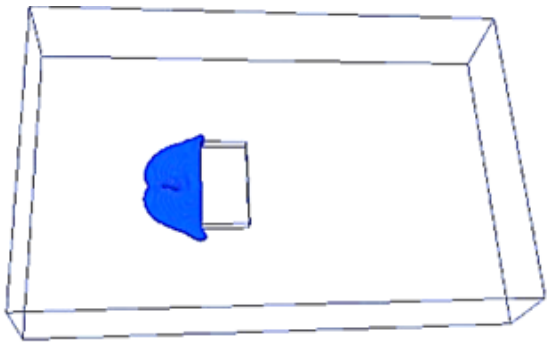

Figure 14. The predicted 2% CO_2 iso-contour at t = 30 s

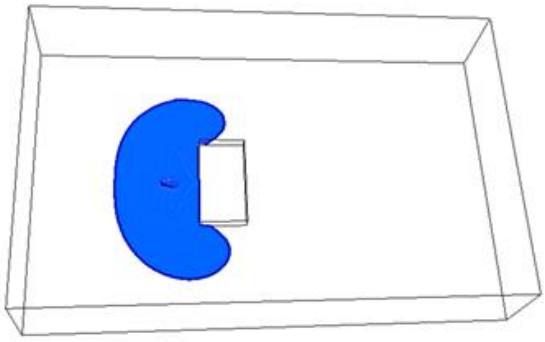

Figure 15. The predicted 2% CO2 iso-contour at t = 300 s

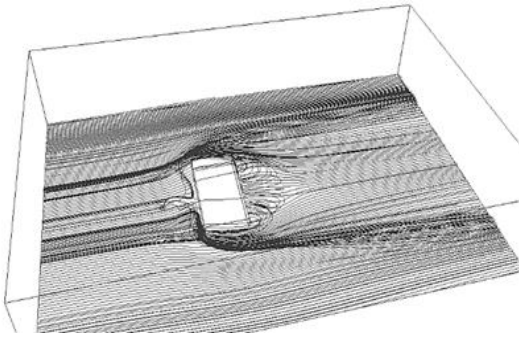

Figure 16. Streamlines around commercial building.

Top-views in Figures 17 and 18, illustrate the horizontal reach of the CO_2 cloud at t = 30 s and t = 5 min, respectively. Iso-concentration contours of 20%, 10% and 7% are observed in the immediate vicinity of the release and form a circular spreading pattern away from the obstacle. However, the building blocks the CO_2 cloud and dilute it at the building edges as the cloud tries to wrap around it.
A cross-wind cut plane view, right after the obstacle (2 m downwind from the obstacle), shown in figure 19 showing only concentrations levels of 0.5% CO_2. A perpendicular view to the former is shown in figure 20. Both help to illustrate the combined blocking/diluting effect of the obstacle. The 0.5% iso-contours only exist to the sides of the building further, and higher concentrations are clearly contained upstream of the building.

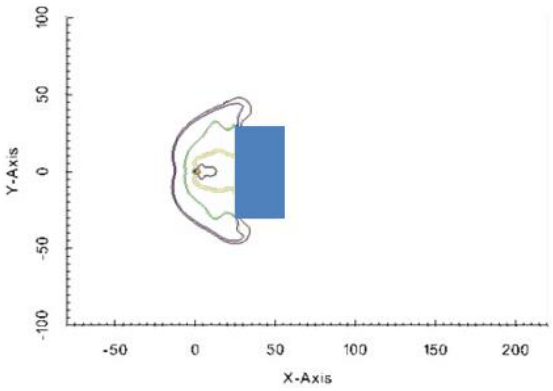

Figure 17. Horizontal CO_2 concentration profile at 1 m height and 30 s. Red: 20 %, black: 10 %, yellow: 7%, green: 4%, blue: 1.5% and brown: 0.5%.

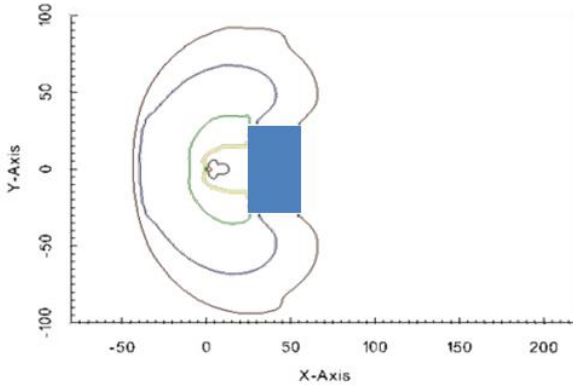

Figure 18. Horizontal CO_2 concentration profile at 1 m height at at t = 5 min. Red: 20 %, black: 10 %, yellow: 7%, green: 4%, blue: 1.5% and brown: 0.5%.

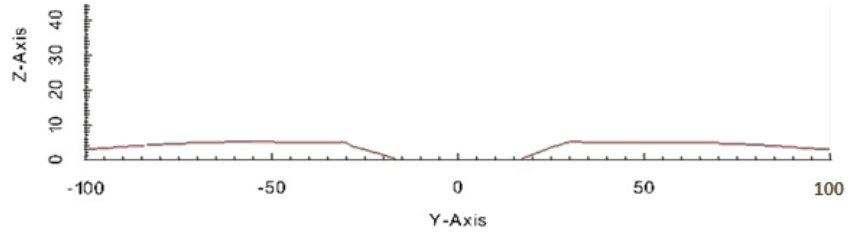

Figure 19. Vertical volume fraction contours at 37 m downwind of the release point at t = 5min. brown: 0.5%.

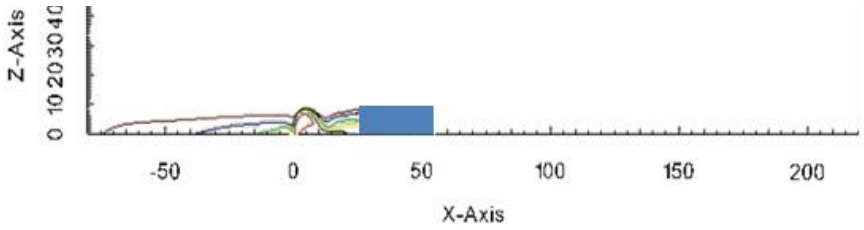

Figure 20. CO_2 iso-contour in the plane x0z at t = 300s. red (inner most): 20%, black: 10%, yellow: 7%, green: 4%, blue: 1.5% and brown: 0.5% (outer most) .

Conclusions

CO_2FOAM, a dedicated solver for CO_2 dispersion previously developed within the frame of the open source CFD code OpenFOAM® by the authors' group has been further extended to include the homogeneous relaxation model which is more suited to account for the presence of solid CO_2 within the release. The code offers both RANS and LES approaches, but only the RANS approach is reported in the present paper. In order to better capture the interaction between the dispersed CO_2 and the ABL-specific boundary layer, a compressible form of the k-ω SST turbulence model is used in conjunction with ABL-specific wall-functions. Predictions have been conducted for Case Study 3 in the COOLTRANS research programme. The CO_2 was released through a puncture in a buried pipe. The numerical simulations used the near-field dispersion studies from Wareing et al. (2014) as input data for the far field dispersion simulation. Evaluations of the different variations of the k-ω SST model suggested that the baseline k-ω SST model delivered the predictions that more closely matched the experimental measurements for the tests cases considered here.

The predictions have achieved reasonable agreement with the data on the basis of a "blind validation", giving confidence to the capability of CO_2FOAM to be used for quantified risk assessment involving far field CO_2 dispersions; especially for situations where screen tests with semi-empirical or integral models suggest more detailed consequence analysis. To illustrate the application of the code, further predictions were conducted using the same release conditions as the baseline case but for scenarios involving a commercial building placed with its front face 25 m downwind of the release. The CO_2 cloud wraps around and passes the building, generating turbulence as well as large flow oscillations and recirculation zones. The increased turbulence level due to the existence of the building would lead to more intense mixing and contribute to the dilution of the CO_2 cloud. This effect is, however, decreased by buoyancy forces as density stratification in the flow tends to suppress turbulence generation. The building has a blocking effect to the flow, where the cloud can be trapped temporarily or diverted towards particular zones.

References

Allason, D., Armstrong, K., Cleaver, P., Halford, A., Barnett, J.,2012. Experimental studies of the behaviour of pressurised release of carbon dioxide. In: IchemE Symposium Series No. 158. IChemE, pp. 142–152.

Apsley, D. D., 2007, CFD calculation of turbulent flow with arbitrary wall roughness, Flow, Turbulence and Combustion, 78:153-175.

Ayrault, M., Simoëns, S. and Méjean, P., 1998, Negative buoyancy effects on the dispersion of continuous gas plumes downwind solid obstacles. J of Hazardous Materials, 57(1–3):79 – 103.

Blocken, B., Carmeliet, J. and Stathopoulos, T., 2007, CFD evaluation of wind speed conditions in passages between parallel buildings—effect of wall-function roughness modifications for the atmospheric boundary layer flow. J of Wind Engineering and Industrial Aerodynamics, 95(9–11), The 4th European and African Conference on Wind Engineering.

Brown, S., Martynov, S., Mahgerefteh, H., and Proust, C., 2007, A Homogeneous Equilibrium Relaxation Flow Model for the Full Bore Rupture of Dense Phase CO2 Pipelines. International Journal of Greenhouse Gas Control, 2013. 17: 349-356.

Cleaver, P., Johnson, M. and Ho, B., 2007, A summary of some experimental data on {LNG} safety. J of Hazardous Materials, 140(3):429 – 438.

Cooper, R., 2012, National Grid's COOLTRANS research programme. J Pipeline Eng; 11: 155–172.

Daish, N. C., Britter, R. E., Linden, P. F. , Jagger, S. F. and Carissimo, B., 2000, Smedis: Scientific model evaluation of dense gas dispersion models. Int. J of Environment and Pollution, 14(1-6):39–51.

Dixon, C.M., Gant, S.E., Obiorah, C. and Bilio, M., 2012, Validation of dispersion models for high pressure carbon dioxide releases. In IChemE Hazards XXIII, pages 153–163, Southport, UK.

Downar-Zapolski, P., Bilicki, Z., Bolle, L., Franco, J., 1996. The non-equilibrium relaxation model for one-dimensional flashing liquid flow. International Journal of Multiphase Flow 22 (3), 473–483.

Engebø, A., Ahmed, N., Garstad, J. J. and Holt, H., 2013, Risk assessment and management for CO2 capture and transport facilities. Energy Procedia, 37(0):2783 – 2793, GHGT-11.

Ferziger, J. H. and Peric, M., 1996, Computational Methods for Fluid Dynamics. Springer-Verlag, Berlin, page 150.

Issa R.I., 1986, Solution of implicitly discretized fluid flow equations by operator-splitting. J. Comput. Phys., 62:40–65.

Patankar S., 1980, Numerical Heat Transfer and Fluid Flow, Hemisphere Publishing Company, page 126.

GL Noble Denton, 2011, Case Study 3-Dense Phase Puncture Experiment, Confidential COOLTRANS Report.

Hanna, S. R., Chang, J. C. and Strimaitis, D. G., 1993, Hazardous gas model evaluation with field observations. Atmos. Environ., 32:3619–3628.

Hsieh, K. J., Lien, F. S. and Yee, E., 2013, Dense gas dispersion modeling of CO_2 released from carbon capture and storage infrastructure into a complex environment. Int. J of Greenhouse Gas Control, 17(0):127 – 139.

Hassid, S., 1983, Turbulent Schmidt number for diffusion models in the neutral boundary layer. Atmospheric Environment, 17: 523-527.

Daly B. J., Harlow F. H., 1970, Transport equations in turbulence. Physics of. Fluids. 13: 2634 – 2649.

Kumar, R. and Dewan, A., 2014, Computational models for turbulent thermal plumes: Recent advances and challenges. Heat Transfer Engineering, 35(4).

Haroun Mahgerefteh, Michael Fairweather, Sam Falle, Jens Melheim, Mathieu Ichard, Idar Storvik, Ole Jacob Taraldset, Trygve Skjold, Ioannis Economu, Dimitrois Tsangaris, Laurence Cusco, Mike Wardman, Simon Gant, Jill Wilday, Yong Chun Zhang, Shaoyun Chen, and Christophe Proust, 2011 , CO_2PIPEHAZ: Quantitative Hazard Assessment for Next Generation CO_2 Pipelines, SYMPOSIUM SERIES NO. 156 Hazards XXII, IChemE.

Maele, K. V. and Merci, B., 2006, Application of two buoyancy-modified – turbulence models to different types of buoyant plumes. Fire Safety J, 41(2):122 – 138.

Sutherland, W., 1893, LII. The viscosity of gases and molecular force. Philosophical Magazine Series 5, 36(223).

Mazzoldi, A., Hill, T. and Colls, J. J., 2011, Assessing the risk for CO_2 transportation within CCS projects, CFD modelling. International Journal of Greenhouse Gas Control, 5(4):816 – 825.

Mazzoldi, A., Hill, T. and Colls, J. J., 2008, CFD and Gaussian atmospheric dispersion models: A comparison for leak from carbon dioxide transportation and storage facilities. Atmospheric Environment, 42(34):8046 – 8054.

McGillivray, A., Saw, J. L., Lisbona, D., Wardman, M. and Bilio, M., 2014, A risk assessment methodology for high pressure CO2 pipelines using integral consequence modelling, Process Safety and Environmental Protection, 92(1):17-26.

Menter, F. R., 1993, Zonal Two Equation k-ω Turbulence Models for Aerodynamic Flows, AIAA Paper 93-2906.
NIST, 1990, JANAF thermochemical tables third edition, Analytical Chemistry, 62(1):48A–48A.
Menter, F. R., 1994, Two-equation eddy-viscosity turbulence models for engineering applications. AIAA J, 32(8).
OpenCFD, 2014, http://www.OpenFOAM®.com.
Parente, A., Gorlé, C., Beeck, J. V. and Benocci, C., 2011, Improved k– model and wall function formulation for the RANS simulation of ABL flows. J of Wind Engineering and Industrial Aerodynamics, 99(4):267 – 278.
Puttock, J.S., 1987, Comparison of thorney island data with predictions of hegabox/hegadas. J of Hazardous Materials, 16(0):439 – 455, Heavy Gas Dispersion Trials at Thorney Island - 2.
Richards, P. J., 1993, Appropriate boundary conditions for computational wind engineering models using the k-ϵ turbulence model, J of Wind Engineering and Industrial Aerodynamics, Vol. 46–47: 145–153.
Richards, P. J. and Hoxey, R. P., 1993, Appropriate boundary conditions for computational wind engineering models using the k-ε turbulence model. J of Wind Engineering and Industrial Aerodynamics, 46–47(0):145 – 153. Proc. the 1st Int. Conf. on Computational Wind Engineering.
Scargiali, F., Grisafi, F., Busciglio, A. and Brucato, A., 2011, Modeling and simulation of dense cloud dispersion in urban areas by means of computational fluid dynamics. J of Hazardous Materials, 197(0):285 – 293.
Wareing, C. J., Woolley, R. M., Fairweather, M., Falle, S.A.E.G. and Cleaver, R.P., 2013a, Large-scale validation of a numerical model of accidental releases from buried CO_2 pipelines. In Andrzej Kraslawski and Ilkka Turunen, editors, 23rd European Symp. on Computer Aided Process Engineering, vol. 32 of Computer Aided Chemical Engineering.
Wareing, C.J., Woolley, R.M., Fairweather, M., and Falle, S.A.E.G., 2013b, A Composite Equation of State for the Modelling of Sonic Carbon Dioxide Jets. American Institute of Chemical Engineers Journal, 59(10): 3928-3942.
Wareing, C.J., Fairweather, M., Falle, S.A.E.G., and Woolley, R.M., 2014a, Modelling punctures of buried high-pressure dense phase CO2 pipelines in CCS applications. International Journal of Greenhouse Gas Control, 29: 231-247.
Wareing, C.J., Fairweather, M., Falle, S.A.E.G., and Woolley, R.M., 2014b, Validation of a Model of Gas and Dense Phase CO2 Jet Releases for Carbon Capture and Storage Application. International Journal of Greenhouse Gas Control, 20: 254-271.
Wareing, C.J., Woolley, R.M., Fairweather, M., Falle, S.A.E.G., and Cleaver, R.P., 2013, Large-Scale Validation of a Numerical Model of Accidental Releases from Buried CO2 Pipelines, in Proceedings of the 23rd European Symposium on Computer Aided Process Engineering - ESCAPE 23, A. Kraslawski and I. Turunen, Editors. Elsevier: Lappeenranta, Finland. p. 229-234.
Webber, D.M., 2011, Generalising two-phase homogeneous equilibrium pipeline and jet models to the case of carbon dioxide. J of Loss Prevention in the Process Industries, 24(4):356 – 360.
Wen, J. X., Heidari, A., Xu, B. P. and Jie, H. J., 2013, Dispersion of carbon dioxide from vertical vent and horizontal releases-A numerical study, Proc IMechE Part E:J Process Mechanical Engineering, 227(2) 125–139, IMechE.
Woolley, R.M., Fairweather, M., Wareing, C.J., Proust, C., Hebrard, J., Jamois, D., Narasimhamurthy, V.D., Storvik, I.E., Skjold, T., Falle, S.A.E.G., Brown, S., Mahgerefteh, H., Martynov, S., Gant, S.E., Tsangaris, D.M., Economou, I.G., Boulougouris, G.C., and Diamantonis, N.I., 2014, An Integrated, Multi-scale Modelling Approach for the Simulation of Multiphase Dispersion from Accidental CO2 Pipeline Releases in Realistic Terrain. International Journal of Greenhouse Gas Control, 27: 221-238.
Zucrow, M.J., Hoffman, J.D., 1975. Gas Dynamics. Wiley, New York.
Frank Huess Hedlund, The extreme carbon dioxide outburst at the menzengraben potash mine 7 July 1953. Safety Science, 50(3):537 – 553, 2012.
Xing, J., Zhenyi Liu, Ping Huang, Changgen Feng, Yi Zhou, Deping Zhang, and Feng Wang. Experimental and numerical study of the dispersion of carbon dioxide plume. Journal of Hazardous Materials, 256–257:40 – 48, 2013.

822 Papanikolaou, E., Heitsch, M., and Baraldi, D., Validation of a numerical code for the simulation of a
823 short-term {CO2} release in an open environment: Effect of wind conditions and obstacles. Journal of
824 Hazardous Materials, 190(1–3):268 – 275, 2011.
825 Pontiggia, M., Derudi, M., Busini, V., and Rota, R., Hazardous gas dispersion: A {CFD} model
826 accounting for atmospheric stability classes. Journal of Hazardous Materials, 171(1–3):739 – 747,
827 2009.
828 Pontiggia, M., Derudi, M., Alba, M., Scaioni, M., and Rota, M., Hazardous gas releases in urban
829 areas: Assessment of consequences through {CFD} modelling. Journal of Hazardous Materials,
830 176(1–3):589 – 596, 2010.